



## Inter-subject Variability in Electric Fields of Motor Cortical tDCS

Ilkka Laakso <sup>a,\*</sup>, Satoshi Tanaka <sup>b</sup>, Soichiro Koyama <sup>d,c</sup>, Valerio De Santis <sup>a</sup>, Akimasa Hirata <sup>a</sup>



<sup>a</sup> Department of Computer Science and Engineering, Nagoya Institute of Technology, Gokiso-cho, Showa-ku, Nagoya 466-8555, Japan

<sup>b</sup> Laboratory of Psychology, Hamamatsu University School of Medicine, Shizuoka 431-3192, Japan

<sup>c</sup> Division of Cerebral Integration, National Institute for Physiological Sciences, Aichi 444-8585, Japan

<sup>d</sup> School of Life Sciences, The Graduate University for Advanced Studies, Kanagawa 240-0193, Japan

### ARTICLE INFO

#### Article history:

Received 3 March 2015

Received in revised form

28 April 2015

Accepted 1 May 2015

Available online 27 May 2015

#### Keywords:

tDCS

Inter-subject variability

Electric field

Finite-element method

Motor cortex

### ABSTRACT

**Background:** The sources of inter-subject variability in the efficacy of transcranial direct current stimulation (tDCS) remain unknown. One potential source of variations is the brain's electric field, which varies according to each individual's anatomical features.

**Objective:** We employed an approach that combines imaging and computational modeling to quantitatively study the extent and primary causes of inter-subject variation in tDCS electric fields.

**Methods:** Anatomically-accurate models of the head and brain of 24 males (age:  $38.63 \pm 11.24$  years) were constructed from structural MRI. Finite-element method was used to computationally estimate the electric fields for tDCS of the motor cortex. Surface-based inter-subject registration of the electric field and functional MRI data was used for group level statistical analysis.

**Results:** We observed large differences in each individual's electric field patterns. However, group level analysis revealed that the average electric fields concentrated in the vicinity of the primary motor cortex. The variations in the electric fields in the hand motor area could be characterized by a normal distribution with a standard deviation of approximately 20% of the mean. The cerebrospinal fluid (CSF) thickness was the primary factor influencing an individual's electric field, thereby explaining 50% of the inter-individual variability, a thicker layer of CSF decreasing the electric field strength.

**Conclusions:** The variability in the electric fields is related to each individual's anatomical features and can only be controlled using detailed image processing. Age was found to have a slight negative effect on the electric field, which might have implications on tDCS studies on aging brains.

© 2015 Elsevier Inc. All rights reserved.

### Introduction

Transcranial direct current stimulation (tDCS) is a non-invasive neuromodulation technique that delivers weak direct currents to the brain through the intact scalp [1,2]. The effects of tDCS depend on the polarity and magnitude of the applied current. For example, the excitability of the primary motor cortex is increased by anodal tDCS and decreased by cathodal tDCS [2–4]. TDCS is appealing for clinical use because it is affordable and mostly well tolerated [5–8].

A major challenge is the large inter-subject variation in the measured outcomes of tDCS [9–11], with about one-half of the subjects failing to respond to the stimulation in the expected

manner [9,11]. Several factors may influence the effectiveness of the tDCS [12,13], but their individual contributions to the inter-subject variations are still unclear. Understanding the individual factors that determine the effectiveness is particularly important if tDCS is to be used clinically because any treatment is expected to have predictable and repeatable effects.

Simulation-based electric field models have been proposed as tools for studying the biophysical mechanisms of tDCS [14], and they could be useful for studying the reasons behind the variations. So far, simulations employing computational models of tDCS have revealed complex patterns of the electric field in individualized anatomically-accurate models of the head and brain [14–24]. However, studies involving tDCS electric-field modeling have so far been limited to only one or very few subjects. The few studies that have used more than one head model have revealed great inter-subject variations in the electric fields, affected by differences in the individual brain anatomy, including that of cerebrospinal fluid [18,24–26]. It can be hypothesized that these variations may be one

This work was partly supported by Konica Minolta Science and Technology Foundation.

\* Corresponding author. Tel./fax: +81 52 735 7916.

E-mail address: [laakso.ilkka@nitech.ac.jp](mailto:laakso.ilkka@nitech.ac.jp) (I. Laakso).

important factor in explaining the experimentally observed variation in the responses to tDCS.

Interpretation, reporting, and visualization of the computational results are not straightforward. Because the morphology of each brain varies greatly, a question arises as to how the variations in the electric fields can be studied. Most authors have reported their modeling results graphically, showing the electric fields on three dimensional brain surfaces, which gives a clear idea regarding the distribution of the electric fields, but makes it difficult to compare the electric fields of two different individuals. Comparison of peak electric field values, which may be important for the safety of tDCS, is not useful either because the peak values may be located at different anatomical sites for different individuals.

Here, we propose that surface-based registration algorithms can be used for analyzing inter-subject variations in tDCS electric fields. Surface-based registration is based on mapping each point on the surface of one brain to that of another so that the anatomical locations of each point are similar on both brain surfaces [27]. First, we use computational modeling to calculate the electric fields of motor cortical tDCS in numerous anatomically-accurate head models. Then, we use the registration techniques to map the electric fields of individual brains to an average template brain, which gives us information on the subject-specific electric fields at each anatomical site. Averaging the electric field over multiple subjects enables us to locate the sites where the electric fields are consistently high despite subject-specific variations. In addition to finding regions with high electric fields, the procedure allows systematic investigation of the extent and causes of inter-subject variability.

## Methods and models

### Imaging methods

High-resolution ( $1 \text{ mm} \times 1 \text{ mm} \times 1 \text{ mm}$ ) T1- and T2-weighted structural MRI scans of seven males (age: 22–32 years) were acquired using a 3.0 T MRI scanner (Verio; Siemens, Ltd., Erlangen, Germany). Functional images of three subjects were acquired for finger-tapping task, in which the subjects tapped with their right index finger. SPM8 software (Wellcome Department of Cognitive Neurology, London, UK) was used for processing and analyzing the functional images [28]. Details of the imaging methods are presented in *Supplementary Material*.

T1- and T2-weighted structural MRIs of additional 20 male subjects (21–55 years) were obtained from a freely available repository (NAMIC: Brain Multimodality, 3.0 T MRI scanner, 1 mm voxel size, available online at <http://hdl.handle.net/1926/1687>). Three of the additional subjects were excluded from further analysis owing to reasons such as poor image quality near the eyes, skull/imaging artefact near the cerebellum, and poor skull–cerebrospinal fluid contrast. In total, the number of subjects was 24 males (age:  $38.63 \pm 11.24$  years).

### Cortical reconstruction and inter-subject registration

Cortical surfaces were reconstructed using the FreeSurfer image analysis software (available online at <http://surfer.nmr.mgh.harvard.edu>). Briefly, FreeSurfer uses the T1-weighted MRI as an input and generates polygonal representations of the grey matter–CSF and white matter–grey matter surfaces [29,30] and creates a variety of surface-based data including maps of cortical curvature and sulcal depth. Then, the cortical folding patterns are used to automatically register the individual's cortical surface to a spherical atlas, producing a mapping that matches the cortical geometry across all the subjects [27]. Here, we apply the mapping for

the registration of computationally generated electric fields. First, the electric fields are calculated for each individual brain, and determined at each vertex of the grey matter surface, as described in “Electric field modeling”. Using the surface-based registration, the vertex electric fields are then mapped to the symmetric *fsaverage\_sym* average brain included in FreeSurfer for statistical analysis and visualization.

### Construction of volume conductor models

A semi-automatic procedure that uses region-growing and thresholding techniques was used to segment the T1- and T2-weighted MRI into distinct tissue categories, each with a different electrical conductivity. Details of the segmentation procedure are presented in the *Supplementary Material*. The conductivity values assigned to each tissue or bodily fluid are listed in *Supplementary Table 1*. All conductivities were assumed to be linear and isotropic.

Briefly, T1- and T2-weighted MRI were first registered and upsampled to a resolution of  $0.5 \text{ mm} \times 0.5 \text{ mm} \times 0.5 \text{ mm}$ . Nervous tissue was segmented into cortical and nuclear grey matter, white matter, cerebellum, and brainstem. The electrical conductivities of major venous sinuses and cerebral veins were assigned to be that of blood. The remaining volume within the skull consisted of CSF and meninges, and its conductivity was assigned based on the estimated proportions of CSF and meningeal tissues in each voxel. The skull was segmented into cortical and cancellous bone. Extracranial soft tissues were assigned the conductivities of muscle, fat, or an average of muscle and fat.

**Figure 1** shows an example of one of the generated anatomical models. The figures of the other 23 models can be found in the *Supplementary Material*. In addition to the 24 individual models, we considered left- and right-mirrored versions of each model, thereby increasing the total number of models studied to 48.

### Electric field modeling

The electric field was determined using the finite-element method with cubical elements and piecewise linear basis functions [31]. Each element corresponds to a 0.5-mm voxel of the volume conductor model. The values of the electric scalar potential at the corners of each cube were considered the degrees of freedom. For visualization and surface-based registration, the electric fields were interpolated linearly on the grey matter surfaces. The interpolation points were located within the grey matter, 0.8 mm below the pial surface. When determining the maximum value of the electric field over a cortical region, the values in the highest  $10 \text{ mm}^2$  area were ignored in order to remove possible numerical errors.

TDCS of the hand area of the left primary motor cortex was modeled. The center of the stimulating electrode was placed at position C3 of the EEG 10/10 System. The input current was 1 mA and the conductivity of the electrodes was 0.3 S/m. The electrodes were circular with an area of  $35 \text{ cm}^2$ . The reference electrode was located above the contralateral orbit (Fp2).

The results were visualized using MATLAB (MathWorks, Inc.). Statistical analysis was performed using the statistics package of GNU Octave. The level of statistical significance was selected as  $P = 0.05$ .

### Definition of anatomical measures

To analyze the causes of inter-subject variation, the correlations between the electric field and twelve subject-specific factors, including the subject's age, were considered. 3D polygonal surfaces were generated from the segmented tissue masks using

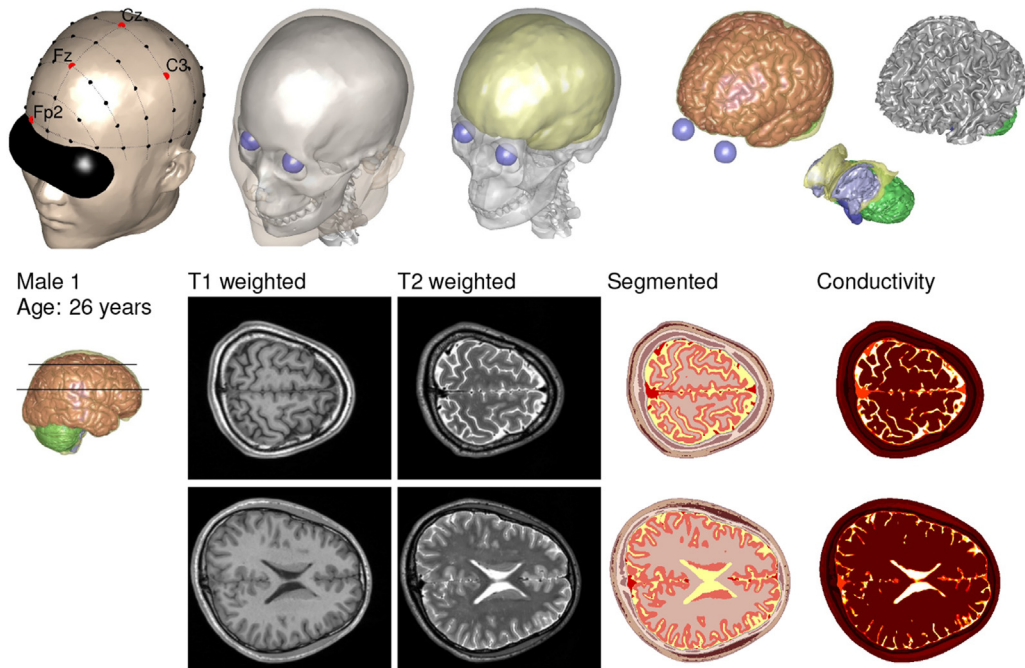


**Figure 1.** Anatomically-accurate model constructed from an MRI. The skin, electrode locations of the EEG 10/10 system, eyes, skull, inner skull boundary, CSF, grey matter, white matter, nuclei, ventricles, and cerebellum are shown. Superior views of the axial slices of the T1- and T2-weighted MRI, final segmented model, and electrical conductivity are also shown.

smoothing and decimation algorithms of the VTK library (available at <http://vtk.org>). As illustrated in Fig. 2, these surfaces were used to automatically determine the head circumference, length and width, electrode distance (the distance between C3 and Fp2 along the scalp surface), region-of-interest (ROI) to inner skull distance, ROI to scalp distance, and skull and scalp thicknesses above the ROI. Additionally, the volumes of the skull and CSF (without ventricles) were determined from the segmented anatomical model, and local sulcal depth (i.e., how deep the point with the maximum electric field in the ROI is located, positive values meaning sulci and negative gyri) was determined using FreeSurfer.

## Results

### Functional imaging

fMRI activation patterns of finger-tapping task performed by three subjects were interpolated on the individual grey matter surfaces obtained using FreeSurfer. All three subjects showed an increased

fMRI activity near the central sulcus. The average fMRI activation pattern was used to select the ROI (Fig. 3, see also Supplementary Fig. 1). The total area of the ROI was  $2.3 \text{ cm}^2$  (on the template brain). The ROI is hereafter referred to as “hand motor area (HMA).”

### Calculated tDCS electric field

Figure 4 shows the electric fields on the grey matter surface of the left hemisphere of 24 subjects. The electric fields for the 24 mirrored subjects are shown in Supplementary Fig. 3. High electric fields were found to be distributed over large regions. It is notable that the site with the maximum electric field was not located within the estimated location of the HMA for any of the subjects.

The inter-subject registration procedure was used to register the individual electric fields of all 48 hemispheres investigated (24 subjects, non-mirrored and mirrored). Figure 5 shows the resulting median electric field overlaid on the template brain.

Figure 5 indicates that, on average, the electric field is strongest in the vicinity of the HMA. The individual electric field hotspots,

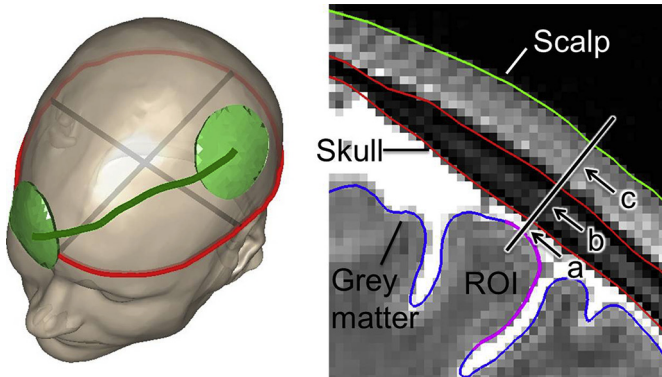


**Figure 2.** Definition of various external and internal distances.

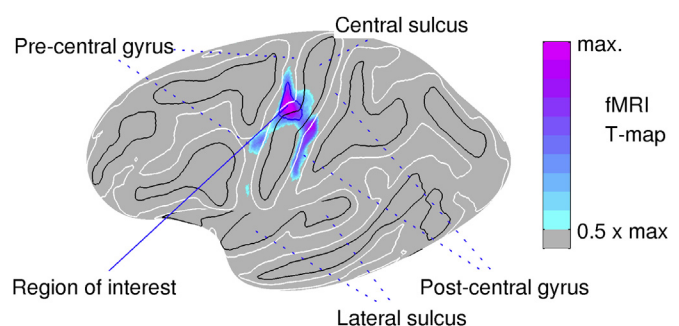


**Figure 3.** Determination of the ROI using surface-based registration of fMRI. Average fMRI activation pattern (three subjects) is shown overlaid on the template brain. Black and white outlines show the extent of the sulci and gyri, respectively.

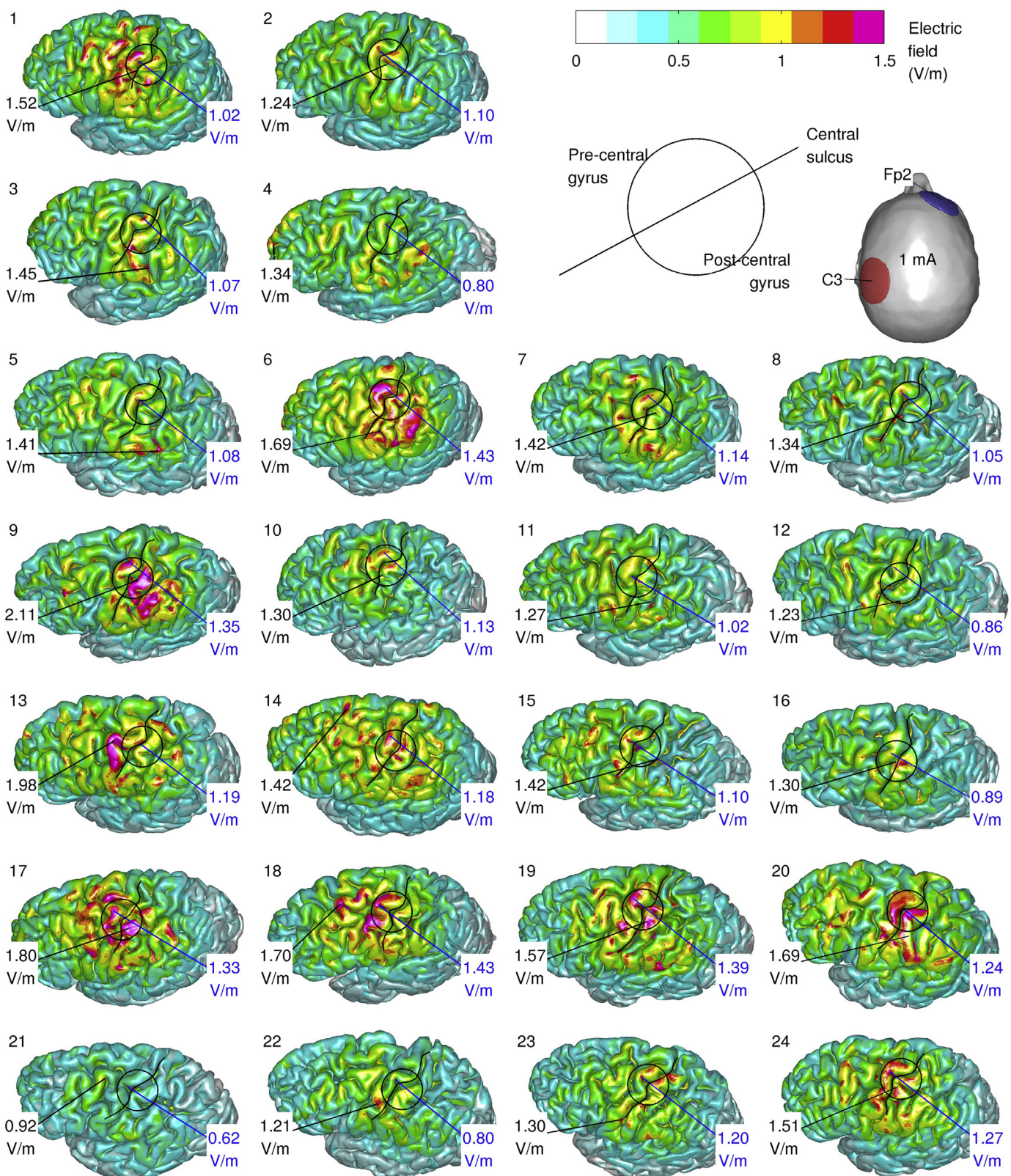


**Figure 4.** Electric fields on the left hemisphere of 24 subjects for tDCS of the motor cortex. The locations and magnitudes of the maximum electric field over the whole hemisphere (black) and maximum electric field in the region of interest (blue) are indicated for each subject. The circle surrounds the vicinity of the hand motor area. The brain surfaces are not drawn to scale. A current of 1 mA is used in the stimulation. (For interpretation of the references to color in this figure legend, the reader is referred to the web version of this article.)

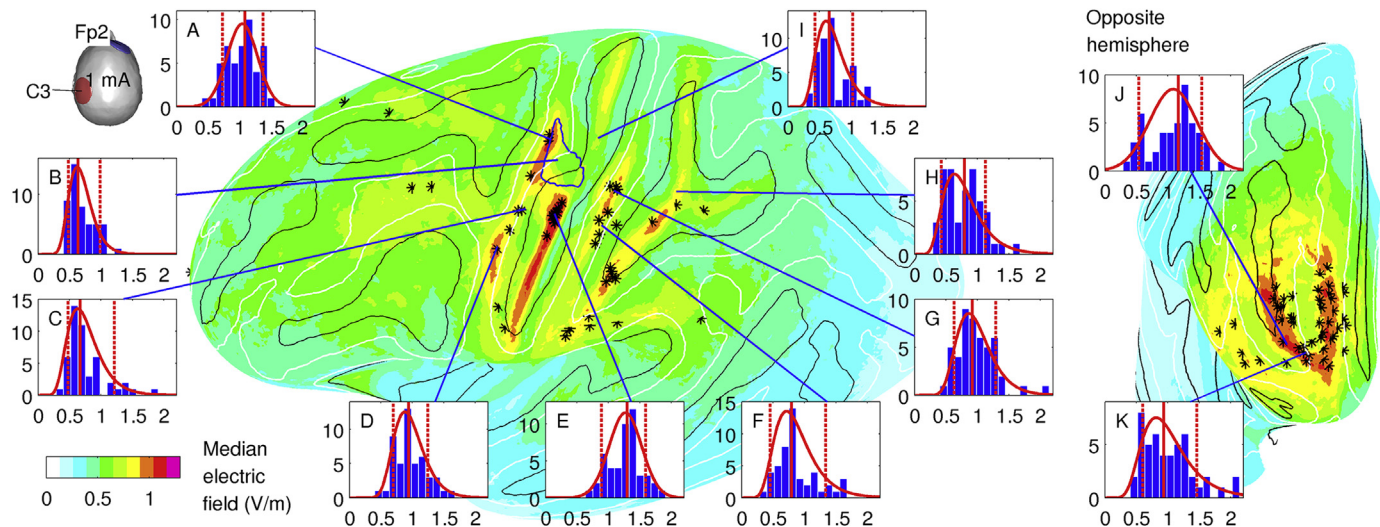


**Figure 5.** Median electric field over 48 hemispheres shown on the template brain. Histogram distributions of electric fields (V/m) are shown at several cortical sites. Probability density functions of the fitted normal or lognormal distributions are superimposed (not to scale). The solid vertical lines are the median values, and the dashed vertical lines indicate the 10th and 90th percentiles. Site A is the location with the highest median electric field within the region of interest, B is the center of the region of interest, E and J are the sites with the highest median value, and F and K are the sites with the largest sample standard deviation. The markers (\*) show the locations of the maximum electric fields of each individual hemisphere.

which may be located far away from the HMA, were suppressed by averaging. This indicates that the hotspots are due to peculiarities of each individual anatomy and they are not common to the population as a whole. At each site or region, not only a different median value but also a different inter-subject distribution of electric fields is evident.

When considering the local brain topology, the electric fields are stronger on the gyral crowns and in the sulcal pits than on the sulcal walls. The highest median electric field was located in the pit of the central sulcus near the HMA. On the opposite hemisphere, the electric fields are distributed in the frontopolar cortex, with no clear distinction between gyral or sulcal sites. The maximum values of the median electric field are comparable on both hemispheres.

#### Variability in calculated electric field

The extent of inter-subject variation in the electric field was investigated by calculating the maximum of each electric field component (absolute value, into brain, out of brain, and along the brain surface) in the HMA. The maximum values of each electric field component can be assumed to be normally distributed (Shapiro–Wilk test for platykurtic samples or Shapiro–Francia test for leptokurtic samples, each  $P > 0.05$ , except for two cases). In addition to the maximum values over the entire HMA, the absolute values of the electric field were analyzed at points A and B shown in Fig. 5. Table 1 lists the summary statistics of each electric field component.

Linear regression was used to analyze the causes of inter-subject variation. Subsequently, we investigated the maximum absolute value of the electric field in the HMA. Scatter plots of the electric fields with the results of the single linear regression analysis for twelve subject-specific factors are shown in Fig. 6.

Figure 6 indicates that there was a strong statistically significant correlation between the electric field in the HMA and the closest distance from the HMA to the inner skull surface ( $R^2 = 0.52$ ,  $P = 10^{-7}$ ). Additionally, there were weak to medium statistically significant negative effects of age ( $R^2 = 0.20$ ,  $P = 0.02$ ), scalp to HMA distance ( $R^2 = 0.16$ ,  $P = 0.04$ ), sulcal depth ( $R^2 = 0.20$ ,  $P = 0.02$ ), and the total CSF volume ( $R^2 = 0.26$ ,  $P = 0.003$ ) on the electric field.

Electrode distance, skull thickness, scalp thickness, external head dimensions (circumference, length, and width), and skull volume did not have a statistically significant effect on the electric field (each  $P \geq 0.7$ ).

#### Discussion

##### Extent of inter-subject variability

In two recent large-scale studies, the responses to tDCS of the motor cortex showed large inter-subject variability [9,11]. Only about one-half of the subjects responded to tDCS in the expected manner, and the subjects could be divided into distinct groups of responders and non-responders [9,11]. In this study, however, the modeled distributions of the individual electric fields showed no clustering to groups with high and low electric fields. Instead, the electric fields in the HMA followed a continuous distribution. Further, in both studies [9,11], the sample standard deviation of the tDCS responses (increase in the amplitude of the motor evoked potential) was larger than the sample mean, indicating a very large range of variation. In contrast, in this study, the standard deviation of the electric field was approximately 20% of the mean (Table 1). These observations indicate that a simple linear relationship between the individual electric fields and the measured responses can

**Table 1**  
Summary statistics of the electric fields in the hand motor area ( $n = 48$ ).

Field component	Mean	(95% C.I.)	S.D.	(95% C.I.)
Absolute value	1.11	(1.05, 1.18)	0.22	(0.18, 0.27)
Into brain	0.97	(0.92, 1.03)	0.20	(0.16, 0.24)
(Out of brain)	-0.04	(-0.11, 0.03)	0.25	(0.21, 0.31)
Along brain	0.88	(0.81, 0.95)	0.24	(0.20, 0.30)
Absolute value, site A	1.04	(0.97, 1.12)	0.24	(0.20, 0.30)
(Absolute value, site B)	0.69	(0.64, 0.75)	0.20	(0.16, 0.25)

Units: V/m per 1 mA current. Sites A (highest median electric field) and B (center of the region of interest) refer to locations shown in Fig. 5. If the site is not given, the values are the maximum values over the entire HMA. The electric field components given in parenthesis are not normally distributed (Shapiro–Francia tests, unadjusted  $P < 0.05$ ).

C.I. = confidence interval, S.D. = standard deviation.

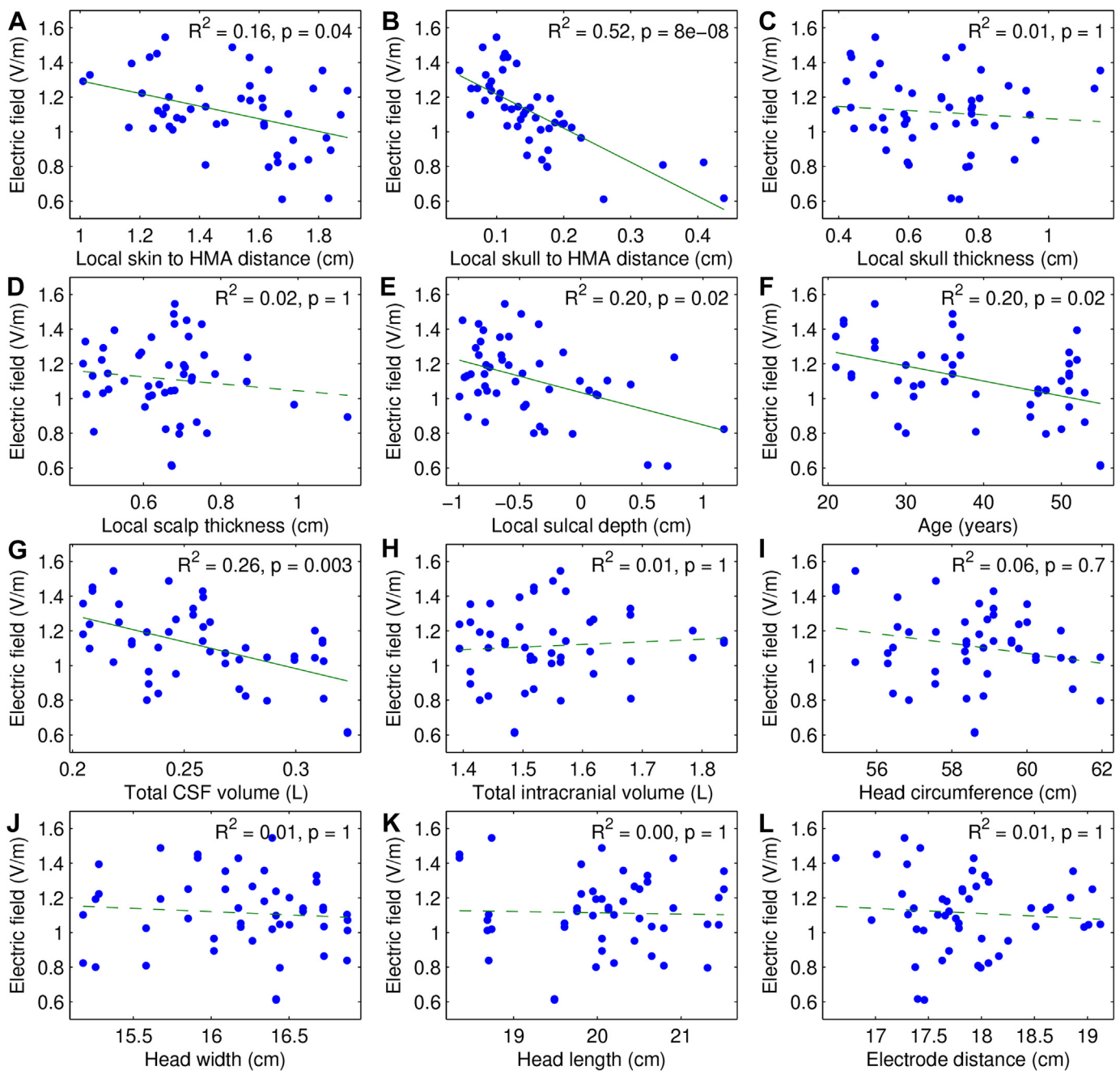


**Figure 6.** Scatter plots of the maximum electric fields in the hand motor area for the C3–Fp2 electrode montage. The best fitting regression lines are superimposed. The  $P$ -values have been adjusted for multiple testing by the Holm–Bonferroni method (number of tests = 12).

only explain a small part of the overall variability. Therefore, if the individual electric field is one of the main factors causing the experimental effects, it must act in a highly nonlinear manner. Alternatively or additionally, we may hypothesize that the experimentally observed responses were caused not by the electric field alone but by its interaction with various neurophysiological factors [8,12,13]. For instance, the cortical region where the electric fields concentrate may exhibit a variable excitability in different individuals.

At the group level, increasing the magnitude of the current or the duration of stimulation monotonically increases the tDCS after-effects when the currents are relatively weak [2], with anodal stimulation increasing the corticospinal excitability and cathodal

stimulation decreasing it [3]. However, for stronger currents, increasing the tDCS current magnitude or stimulation duration does not always result in an increase in its efficacy but may even change the direction of effects [32], suggesting that there must be a complex non-monotonic relationship between the electric field and the resulting effects. Consequently, fully understanding the extent of the inter-subject variability in responses that is caused by the variability in the individual electric fields would require information about the current magnitude–response characteristics at the individual level. For example, the electric fields in our study had a relative standard deviation of approximately 20%, depending on where and which component of the electric field was studied (Table 1). Hypothetically, the impact this variability has on the

measured responses could be approximated by measuring the change in responses at the individual level when the stimulation current is altered by  $\pm 20\%$ . To the best of our knowledge, there have been no studies on this subject.

### Reasons for variability

We found that the distance from the HMA to the inner boundary of the skull was the most important single factor affecting the calculated electric fields, explaining about one-half of the variation in the subject-specific electric fields. This distance is related to the thickness of the CSF, and it is determined by both the total volume of the CSF and the individual cortical morphology of the HMA. A thicker layer of CSF above the HMA results in a weaker electric field. A previous modeling study [24] found that the CSF and skull thicknesses were the main determinants of the electric field, explaining more than half of the intra-subject variation caused by electrode positioning. Our results for inter-subject variation are similar, but the skull thickness did not have a statistically significant effect on the electric field. The thickness and volume of CSF and cortical morphology can only be measured using imaging techniques, suggesting that there may not be a simple method for estimating the tDCS electric field based only on external features. Therefore, if a tDCS study does not feature detailed image processing, variations in the individual electric fields are mostly uncontrollable. However, we observed a slight negative effect ( $R^2 = 0.2$ ) of age on the electric field. This effect was due to a positive correlation between age and the volume of CSF [33] (in the present study:  $n = 24$ ,  $R^2 = 0.49$ ,  $P = 0.0001$ ). Except for age, other readily available measures, such as skull size or external head dimensions, did not have a significant effect on the electric field.

The effect of age on the electric field is important because there already is experimental evidence of age affecting the outcomes of tDCS [34–36]. These studies featured groups of elderly subjects (mean ages older than 60 years) whose responses to anodal tDCS of the primary motor cortex [35,36] or dorsolateral prefrontal cortex [34] were compared to similar responses of younger subjects (mean ages under 25 years). It is notable that studies with large groups of young subjects have not revealed significant effects of age on motor cortical tDCS [9,11]. Our results suggest that the difference in responses between age groups may at least partially originate from the difference in electric fields. For instance, extrapolating using the linear regression model (Fig. 6), a group with an average age of 60 years would have a 30% weaker group average electric field than a group with an average age of 20 years. When analyzing the effects of age on tDCS, it is important to consider that the dosage, i.e., the brain electric field, may differ between age groups even for otherwise identical experimental configurations.

### Which sites are modulated by tDCS?

In addition to the measures of variability, the group average data provide information about the sites where the electric fields are consistently high despite subject-specific variations. These data are useful for determining the most probable sites affected by tDCS.

We observed that the electric field hotspot was typically not located in the hand area of the primary motor cortex in individual brains, which is consistent with the findings of previous computational modeling studies [18,25]. However, after inter-subject registration and averaging, the group average electric field was found to be the strongest near the HMA. Individual electric field hotspots far away from the target area vanished when the averaging procedure was applied, suggesting that they were not common to

the population as a whole, and thus, unlikely to be a cause of (group level) responses to tDCS. Therefore, we can hypothesize that tDCS modulates the cortical excitability directly in the primary motor cortex.

However, the electric fields were also consistently high in the pit of the central sulcus (Brodmann area 3a) and on the apex of the post–central gyrus (Brodmann area 1). Hence, on the basis of the group average electric field data, we cannot exclude the possibility of simultaneous modulation of the somatosensory areas. These areas may exhibit larger variations in the electric fields than the HMA (Fig. 5), which may be important if connections from these or other areas to the primary motor cortex were to play a role in tDCS variability.

### Limitations

There is a large range of uncertainty in the *in vivo* electrical properties of tissue. Here, the modeled electric fields were higher (peak median 1.2 V/m) than the values of 0.3–0.4 V/m obtained previously [18,25,26]. When the simulations were repeated for a higher brain and scalp conductivity, the electric fields were comparable with previous studies (Supplementary Fig. 4). Even with different conductivity values, the sites with the highest average electric fields were located in the vicinity of the HMA. Also, the relative variability of the electric field in the HMA was not affected by the conductivity.

The separation between the cortex and skull may strongly affect the electric fields. Here, we used surface-based segmentation for the brain and upsampled the MRI to a resolution of 0.5 mm to segment the skull and CSF. The process may include uncertainty especially for subjects with a very short cortex–skull distance. Another limitation is that we did not model anisotropy conductivity of the white matter [19,37]. Possible inter-individual variations in the anisotropy could widen the variation range of the electric fields.

### Conclusion

We applied a surface-based registration method for inter-subject analysis of computational electric field data. The procedure allows investigation of the tDCS electric fields at a group level rather than at single subject level, and it can be applied to study the extent and main causes of inter-subject variation in the individual electric fields.

Individual electric fields showed variations in magnitudes and inconsistent locations of the electric field hotspots. Despite this, the highest group average fields concentrated in the vicinity of the primary motor cortex. Variations in the electric field, investigated in the hand area of the motor cortex, can potentially explain some of the variability in tDCS experimental responses. However, the full significance of the variations is uncertain without better knowledge about strength–response characteristics of tDCS.

The variations in the electric fields are mainly caused by differences in the individual morphology of the CSF and brain, and hence, cannot be controlled in experimental studies unless detailed image processing is performed. The sole external factor that had a significant effect on the electric field was age, which may have implications for tDCS studies of the aging brain.

### Appendix. Supplementary data

Supplementary data related to this article can be found online at <http://dx.doi.org/10.1016/j.brs.2015.05.002>.

## References

- [1] Priori A, Berardelli A, Rona S, Accornero N, Manfredi M. Polarization of the human motor cortex through the scalp. *Neuroreport* 1998;9(10):2257–60.
- [2] Nitsche MA, Paulus W. Excitability changes induced in the human motor cortex by weak transcranial direct current stimulation. *J Physiol (Lond)* 2000;527(Pt 3):633–9.
- [3] Nitsche MA, Paulus W. Sustained excitability elevations induced by transcranial DC motor cortex stimulation in humans. *Neurology* 2001;57(10):1899–901.
- [4] Furubayashi T, Terao Y, Arai N, et al. Short and long duration transcranial direct current stimulation (tDCS) over the human hand motor area. *Exp Brain Res* 2008;185(2):279–86.
- [5] Fregni F, Pascual-Leone A. Technology insight: noninvasive brain stimulation in neurology—perspectives on the therapeutic potential of rTMS and tDCS. *Nat Clin Pract Neurol* 2007;3(7):383–93.
- [6] Hummel FC, Celnik P, Pascual-Leone A, et al. Controversy: noninvasive and invasive cortical stimulation show efficacy in treating stroke patients. *Brain Stimul* 2008;1(4):370–82.
- [7] Tanaka S, Watanabe K. Transcranial direct current stimulation—a new tool for human cognitive neuroscience. *Brain Nerve* 2009;61(1):53–64.
- [8] Brunoni AR, Nitsche MA, Bolognini N, et al. Clinical research with transcranial direct current stimulation (tDCS): challenges and future directions. *Brain Stimul* 2012;5(3):175–95.
- [9] López-Alonso V, Cheeran B, Rio-Rodríguez D, Fernández-Del-Olmo M. Inter-individual variability in response to non-invasive brain stimulation paradigms. *Brain Stimul* 2014;7(3):372–80.
- [10] Tremblay S, Lepage JF, Latulipe-Loiselle A, Fregni F, Pascual-Leone A, Théoret H. The uncertain outcome of prefrontal tDCS. *Brain Stimul* 2014;7(6):773–83.
- [11] Wiethoff S, Hamada M, Rothwell JC. Variability in response to transcranial direct current stimulation of the motor cortex. *Brain Stimul* 2014;7(3):468–75.
- [12] Ridding MC, Ziemann U. Determinants of the induction of cortical plasticity by non-invasive brain stimulation in healthy subjects. *J Physiol (Lond)* 2010;588(Pt 13):2291–304.
- [13] Krause B, Cohen Kadosh R. Not all brains are created equal: the relevance of individual differences in responsiveness to transcranial electrical stimulation. *Front Syst Neurosci* 2014;8:25.
- [14] Datta A, Bansal V, Diaz J, Patel J, Reato D, Bikson M. Gyri-precise head model of transcranial direct current stimulation: Improved spatial focality using a ring electrode versus conventional rectangular pad. *Brain Stimul* 2009;2(4):201–7.
- [15] Parazzini M, Fiocchi S, Rossi E, Paglialonga A, Ravazzani P. Transcranial direct current stimulation: estimation of the electric field and of the current density in an anatomical human head model. *IEEE Trans Biomed Eng* 2011;58(6):1773–80.
- [16] Neuling T, Wagner S, Wolters CH, Zaehle T, Herrmann CS. Finite element model predicts current density distribution for clinical applications of tDCS and tACS. *Front Psychiatry* 2012;3:83.
- [17] Datta A, Zhou X, Su Y, Parra LC, Bikson M. Validation of finite element model of transcranial electrical stimulation using scalp potentials: implications for clinical dose. *J Neural Eng* 2013;10(3):036018.
- [18] Truong DQ, Magerowski G, Blackburn GL, Bikson M, Alonso-Alonso M. Computational modeling of transcranial direct current stimulation (tDCS) in obesity: Impact of head fat and dose guidelines. *Neuroimage Clin* 2013;2:759–66.
- [19] Shahid SS, Bikson M, Salman H, Wen P, Ahfock T. The value and cost of complexity in predictive modelling: role of tissue anisotropic conductivity and fibre tracts in neuromodulation. *J Neural Eng* 2014;11(3):036002.
- [20] Wagner S, Rampersad SM, Aydin Ü, et al. Investigation of tDCS volume conduction effects in a highly realistic head model. *J Neural Eng* 2014;11(1):016002.
- [21] Noetscher GM, Yanamadala J, Makarov SN, Pascual-Leone A. Comparison of cephalic and extracephalic montages for transcranial direct current stimulation—a numerical study. *IEEE Trans Biomed Eng* 2014;61(9):2488–98.
- [22] Kim JH, Kim DW, Chang WH, Kim YH, Kim K, Im CH. Inconsistent outcomes of transcranial direct current stimulation may originate from anatomical differences among individuals: electric field simulation using individual MRI data. *Neurosci Lett* 2014;564:6–10.
- [23] Parazzini M, Fiocchi S, Liorni I, Priori A, Ravazzani P. Computational modeling of transcranial direct current stimulation in the child brain: implications for the treatment of refractory childhood focal epilepsy. *Int J Neural Syst* 2014;24(2):1430006.
- [24] Opitz A, Paulus W, Will S, Antunes A, Thielscher A. Determinants of the electric field during transcranial direct current stimulation. *Neuroimage* 2015;109:140–50.
- [25] Datta A, Truong D, Minhas P, Parra LC, Bikson M. Inter-individual variation during transcranial direct current stimulation and normalization of dose using MRI-derived computational models. *Front Psychiatry* 2012;3:91.
- [26] Bai S, Dokos S, Ho KA, Loo C. A computational modelling study of transcranial direct current stimulation montages used in depression. *Neuroimage* 2014;87:332–44.
- [27] Fischl B, Sereno MI, Tootell RB, Dale AM. High-resolution intersubject averaging and a coordinate system for the cortical surface. *Hum Brain Mapp* 1999;8(4):272–84.
- [28] Friston KJ. Functional and effective connectivity in neuroimaging: a synthesis. *Hum Brain Mapp* 1994;2(1–2):5678.
- [29] Dale AM, Fischl B, Sereno MI. Cortical surface-based analysis. i. segmentation and surface reconstruction. *Neuroimage* 1999;9(2):179–94.
- [30] Fischl B, Dale AM. Measuring the thickness of the human cerebral cortex from magnetic resonance images. *Proc Natl Acad Sci U S A* 2000;97(20):11050–5.
- [31] Laakso I, Hirata A. Fast multigrid-based computation of the induced electric field for transcranial magnetic stimulation. *Phys Med Biol* 2012;57(23):7753–65.
- [32] Batsikadze G, Moliadze V, Paulus W, Kuo MF, Nitsche MA. Partially non-linear stimulation intensity-dependent effects of direct current stimulation on motor cortex excitability in humans. *J Physiol (Lond)* 2013;591(Pt 7):1987–2000.
- [33] Good CD, Johnsrude IS, Ashburner J, Henson RN, Friston KJ, Frackowiak RS. A voxel-based morphometric study of ageing in 465 normal adult human brains. *Neuroimage* 2001;14(1 Pt 1):21–36.
- [34] Boggio PS, Ferrucci R, Rigonatti SP, et al. Effects of transcranial direct current stimulation on working memory in patients with Parkinson's disease. *J Neurol Sci* 2006;249(1):31–8.
- [35] Fujiyama H, Hyde J, Hinder MR, et al. Delayed plastic responses to anodal tDCS in older adults. *Front Aging Neurosci* 2014;6:115.
- [36] Heise KF, Niehoff M, Feldheim JF, Liuzzi G, Gerloff C, Hummel FC. Differential behavioral and physiological effects of anodal transcranial direct current stimulation in healthy adults of younger and older age. *Front Aging Neurosci* 2014;6:146.
- [37] Suh HS, Lee WH, Kim TS. Influence of anisotropic conductivity in the skull and white matter on transcranial direct current stimulation via an anatomically realistic finite element head model. *Phys Med Biol* 2012;57(21):6961–80.